5th ECCOMAS Thematic Conference on
Computational Methods in Structural Dynamics and Earthquake Engineering
M. Papadrakakis, V. Papadopoulos, V. Plevris (eds.)
Crete Island, Greece, 25–27 May 2015

SEISMIC FRAGILITY ANALYSIS OF EXISTING URM BUILDINGS: A STUDY ON KATHMANDU VALLEY

Sujan Shrestha[1], Lorenzo Colarusso[2], Domenico Liberatore[3] and Daniela Addessi[4]

[1] Dept. of Structural and Geotechnical Engineering, Sapienza University of Rome
Via Antonio Gramsci 53, 00197 Rome, Italy
e-mail: suzan_sth@yahoo.com

[2] Dept. of Structural and Geotechnical Engineering, Sapienza University of Rome
Via Eudossiana 18, 00184 Rome, Italy
e-mail: lorencola@gmail.com

[3] Dept. of Structural and Geotechnical Engineering, Sapienza University of Rome
Via Antonio Gramsci 53, 00197 Rome, Italy
e-mail: domenico.liberatore@uniroma1.it

[4] Dept. of Structural and Geotechnical Engineering, Sapienza University of Rome
Via Eudossiana 18, 00184 Rome, Italy
e-mail: daniela.addessi@uniroma1.it

Keywords: URM walls, Equivalent Frame Model, Capacity Spectrum Method, Fragility Curves.

Abstract. *Seismic fragility analysis is performed for the assessment of in-plane mechanisms of existing unreinforced masonry (URM) buildings of Kathmandu Valley. The equivalent frame model is used, which has been validated by analyzing the URM prototype tested at the University of Pavia and comparing the analytical results with the experimental outcomes. Existing URM buildings of Kathmandu Valley are firstly investigated by means of a Rapid Visual Screening survey, and the most representative buildings are selected as prototypes for the analysis. Monte Carlo simulation method is used to account for the uncertainty of the mechanical parameters of each prototype. Analyses are carried out both with correlated and uncorrelated distributions of uncertain parameters. Finally, fragility curves are calculated in terms of spectral displacement, according to the capacity spectrum method.*

1 INTRODUCTION

Nepal has a long seismic history due to its location on a very active tectonic zone. Three main fault lines, each running East to West, are causes of major earthquakes in Nepal: the main central thrust (MCT) at the foot of the greater Himalaya joining the midland mountains, the main boundary thrust (MBT) at the junction of the lesser Himalaya and the Siwalik, and the main frontal thrust (MFT) south of the Siwalik [ICIMOD, 2007]. These fault lines are the result of the subduction of the Indian plate under the Eurasian Plate (Figure 1).

Major earthquakes were reported in 1255 AD, 1810 AD, 1866 AD, 1934 AD, 1980 AD and 1988 AD. In 1934, the fault line that runs beneath the Kathmandu valley slipped causing a M 8.4 earthquake which destroyed more than 80,000 buildings and claimed 8,500 lives [United Nation Office for the Coordination of the Humanitarian Affairs (OCHA), 2013]. It was the last major earthquake which shook the city of Kathmandu and the surrounding valley. One of the most detailed studies may be found in the field memoir published by the Geological Survey of India [Jain, 1998].

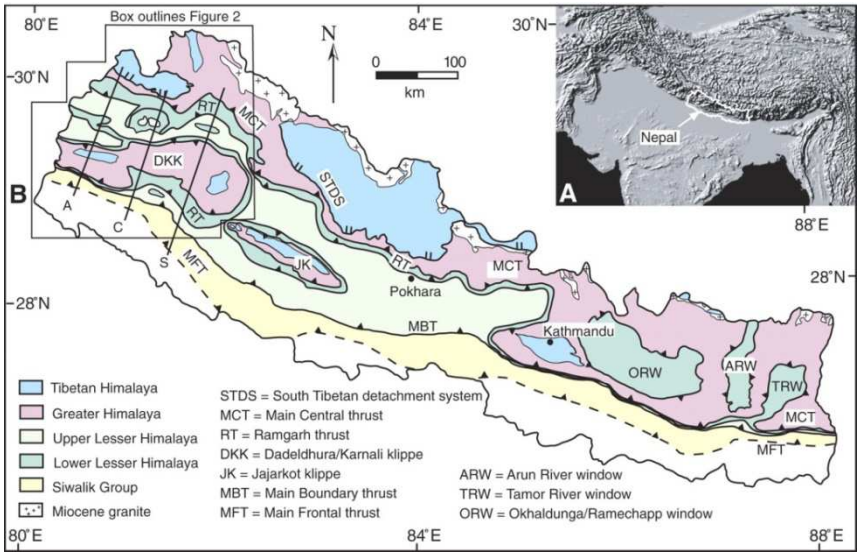

Figure 1: Major thrusts of Nepal (source: http://geosphere.gsapubs.org).

In Nepal, unreinforced brick masonry (URM) construction is the most common type in the historical sites of Kathmandu Valley. UNESCO has already included the historical centres of the three cities (Kathmandu, Bhaktapur, Lalitpur) of Kathmandu Valley into the World Heritage Sites. These sites are enriched with their unique architectural heritage, palaces, temples and courtyards with a symbiosis of Hinduism, Buddism and Tantrism, built between the 12th and the 18th centuries by the ancient Malla kings of Nepal.

Several studies on loss estimations have been carried out for the Kathmandu Valley. Two of such studies are the "Kathmandu Valley Earthquake Risk Management Project" (KVERMP, 1999) and the "Study on earthquake disaster mitigation in the Kathmandu valley, Kingdom of Nepal" carried out in 2002 by the Japan International Cooperation Agency (JICA) and the Ministry of Home Affairs, HMG of Nepal, 2002. Both studies estimate the damage to the buildings and the casualties in the case of repetition of the 1934 earthquake.

However, the definition of the building classes is not completely clear in these studies, as well as the mechanical properties of building materials. The Department of Survey categorizes the buildings into four classes, namely permanent, semi-permanent, temporary and other. Thus, it is difficult to develop fragility curves for such types of buildings.

Today, Kathmandu is a city completely different from that almost levelled in 1934. It has almost 3.0 million inhabitants, many living and working in buildings that will not withstand a significant seismic event. The present study is focused on the systematic categorization of the existing URM buildings, and investigates their in-plane response by means of static nonlinear analysis. Different uncertainty parameters regarding the mechanical properties of unreinforced masonry are considered, and the results are used to develop fragility curves in terms of spectral displacement.

2 EQUIVALENT FRAME MODEL

As shown by recent earthquakes [Penna *et al.*, 2014], [Sorrentino *et al.*, 2014a,b], when the masonry walls are properly constrained by horizontal structures and toothed with orthogonal walls, out-of-plane mechanisms are prevented and in-plane mechanisms can develop.

An equivalent frame model is commonly used by different authors [Magenes and Della Fontana, 1998], [Salonikios *et al.*, 2003], [Kappos *et al.*, 2006], [Pasticier *et al.*, 2008] for the analysis of nonlinear in-plane response of unreinforced masonry walls under horizontal seismic actions. A finite element model is used to define the equivalent frame model, consisting of vertical elements (piers) and horizontal elements (spandrels) (Figure 2). Intersection zones are considered rigid and the effective height of the piers is calculated using the formulation provided by [Dolce, 1991] (Figure 3):

$$H_{eff} = h' + \frac{1}{3h'} D\left(H - h'\right) \tag{1}$$

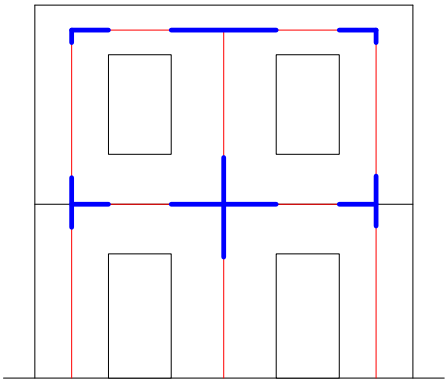

Figure 2: Equivalent frame model.

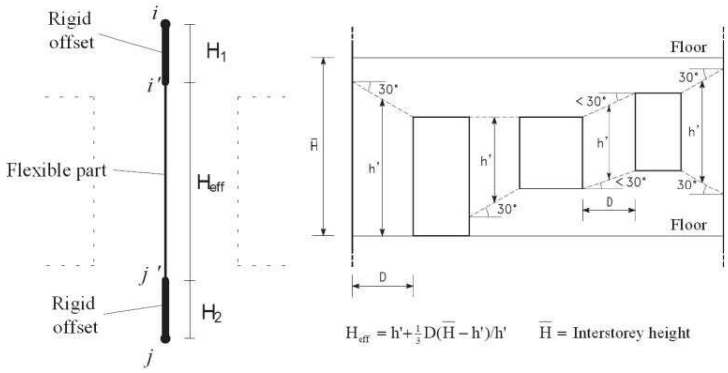

Figure 3: Effective height of piers [Dolce, 1991].

The finite element proposed by [Addessi *et al.*, 2015], [Liberatore and Addessi, 2015] is used in this study. The lumped hinge approach has been adopted in order to model the nonlinear constitutive response of masonry, introducing two flexural hinges at the ends of the element, together with a shear link, with elastic-perfectly plastic behavior (Figure 4).

The finite element is validated by comparing the numerical results on Pavia prototype door wall D with the experimental outcomes [Calvi and Magenes, 1994], [Calvi and Magenes, 1995]. The prototype consists of a two storey wall, with two door openings at the first level and two window openings at the second level (Figure 5).

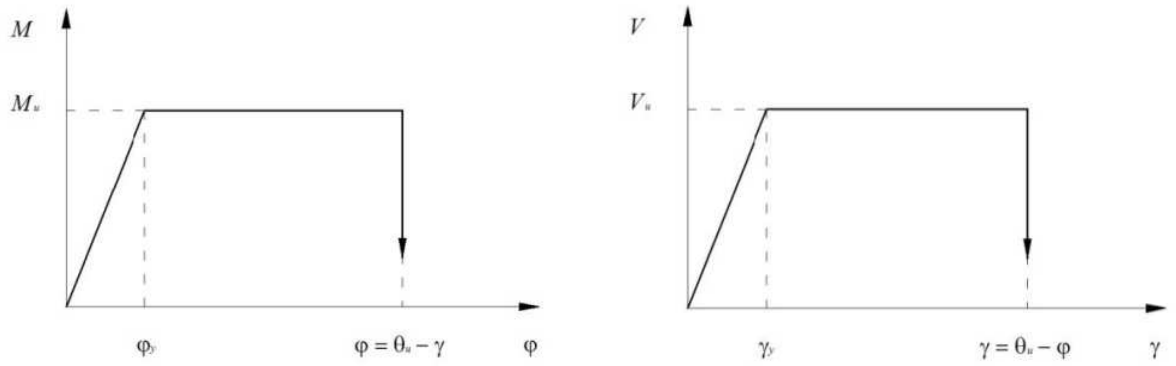

a) Flexural response b) Shear response

Figure 4: Elastic-perfectly plastic behaviour of flexural hinges and shear link.

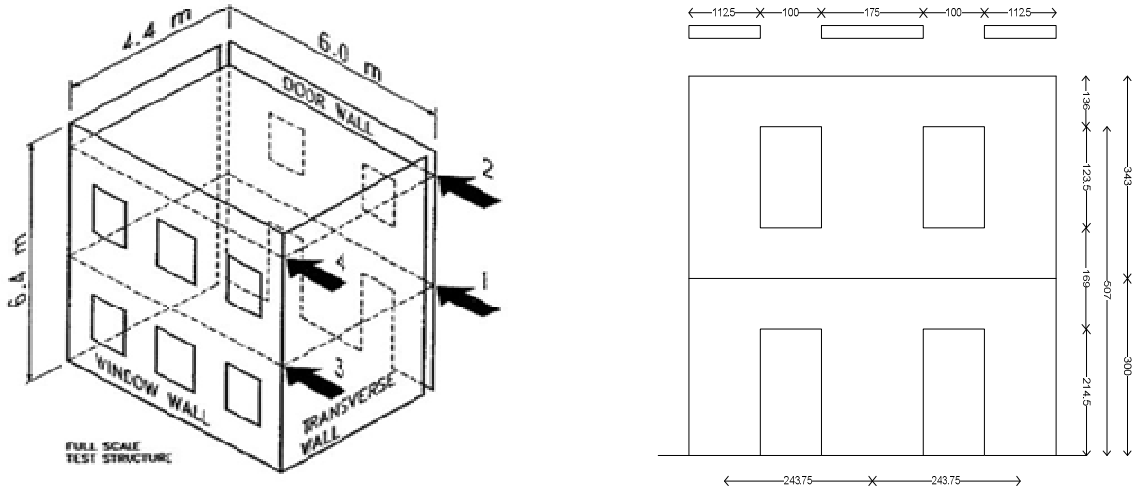

a) 3D model of the Pavia prototype b) Pavia door wall D

Figure 5: Geometric configuration of Pavia prototype.

Two uniformly distributed vertical loads are applied at the floor levels. The structural model is subjected to increasing lateral loads, applied at the floor levels, keeping 1:1 ratio between the loads at the first and second floor. In order to follow the softening branches, an external rigid vertical beam is introduced, hinged to the ends of the floors. The analysis is performed by controlling the displacement at the mid-point of the beam, which shares the reactive force in equal parts to the first and second floor.

The mechanical properties, based on the available experimental tests, are reported in Table 1. The FE model of wall D is shown in Figure 6.

E (MPa)	**G (MPa)**	**f_m (kN/m^2)**	**f_{vk}(kN/m^2)**
1900	500	2000	69.3

Table 1: Mechanical properties for Pavia door wall D.

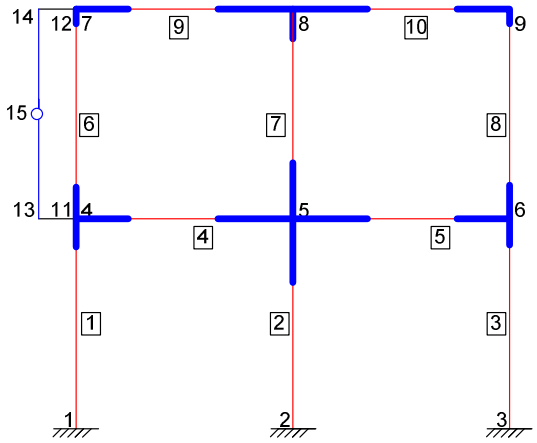

Figure 6: FE model of wall D.

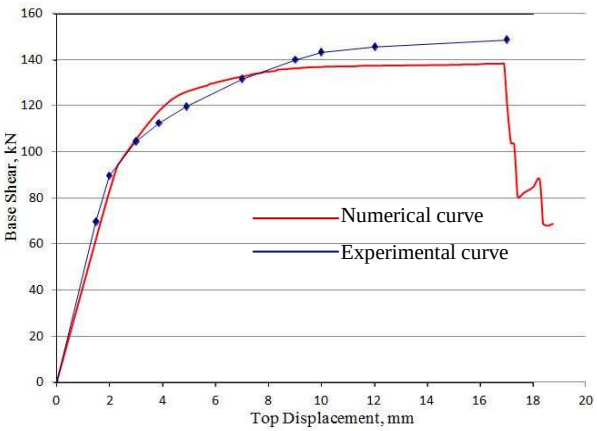

Figure 7: Experimental vs. numerical pushover curve.

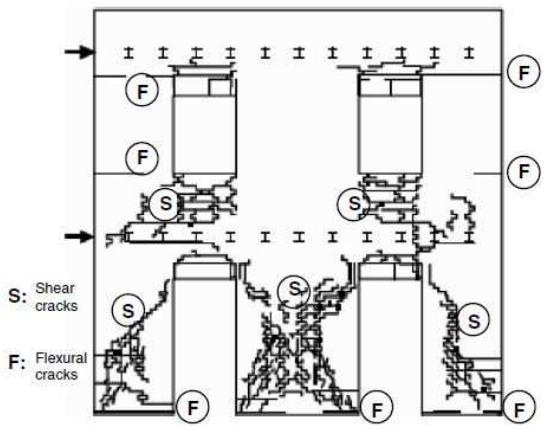

Figure 8: Crack formation from test result.

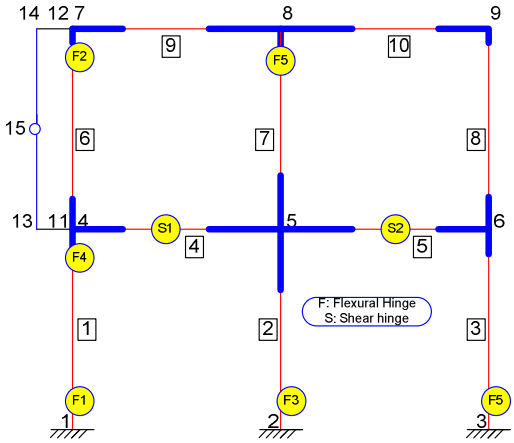

Figure 9: Hinge formation in analytical result.

The comparison between the numerical pushover curve and the experimental envelope curve, reported in Figure 7, shows a good agreement. For further verification of the results, the experimental crack pattern at drift 0.4% (Figure 8) is compared with the formation of hinges in the numerical model (Figure 9), showing again a satisfactory agreement.

3 ANALYSIS OF URM BUILDINGS OF KATHMANDU VALLEY

A preliminary survey was carried out in Bode, one of the historic cities of Kathmandu Valley, located in Madhyapur Thimi Municipality, Bhaktapur, according to the Rapid Visual Screening Method [FEMA, 2002]. Different structural and nonstructural parameters (e.g. storey's number, inter-storey height, materials, openings, age, dimensions of walls, observed damage, number of residents, etc.) of nearly 300 URM buildings were collected, and the buildings were grouped into different classes. Nine prototype walls are selected for the analysis, with storey's number ranging between 2 and 4 (2S, 3S, 4S) and bay's number ranging between 1 and 3(1B, 2B, 3B) (Figure 10).

The uncertainties associated with the mechanical properties of brick masonry are taken into account by deriving a set of variants using Monte Carlo simulation [Rota *et al.*, 2010], [CNR, 2014] The associated mean material properties and coefficients of variation, taken from

literature studies [Jaishi *et al.*, 2003], [Parajuli *et al.*, 2011a,b], [Parajuli *et al.*, 2012], [Parajuli, 2012], are reported in Table 2.

Parameter	Mean	St. Dev.	CoV	Lower bound	Upper bound
E (MPa)	509	101.8	20%	341.55	676.45
G (MPa)	204	40.8	20%	136.89	271.11
f_c (kN/m^2)	1820	364	20%	1221.27	2418.73
f_{v0} (kN/m^2)	100	20	25%	67.10	132.89
drift$_{sh}$ (%)	0.4	–	–	–	–
drift$_{fl}$ (%)	0.6	–	–	–	–

Table 2: Mechanical parameters of masonry adopted for the analysis.

Assuming that the mechanical parameters follow a normal distribution, 30 models of each prototype are generated for Monte Carlo analysis. The analysis has been conducted assuming either correlated or uncorrelated distributions of the parameters. As an example, the pushover curves for 2S2B wall under the hypotheses of correlated and uncorrelated distributions are shown in Figure 11. It has been seen that all pushover curves follow almost the same pattern in the case of correlated distributions, whereas they follow independent patterns, with higher scatter, in the case of uncorrelated distributions. Uncorrelated distributions of mechanical parameters are believed to provide more realistic results.

The original pushover curves are converted into capacity spectrum curves, where spectral acceleration (S_a) is plotted vs. spectral displacement (S_d), according to the AD format [ATC, 1996]. The displacement shape, normalized to top displacement, is shown in Figure 12 for different storey's numbers.

Figure 13 shows the capacity curves bi-linearized according to [ATC, 1996], i.e. equalling the area under the bilinear curve to that of the effective capacity curve, and assuming the same initial stiffness. It can be observed that the effect of the variation of storey's number is predominant compared to bay's number. Furthermore, the yielding spectral acceleration is lower for higher storey's number, due to the increase of seismic loads caused by the greater weight of the wall. The numerical values corresponding to the yield point and the ultimate point are shown in Table 3.

4 FRAGILITY CURVES

The fragility curve represents the conditional probability of being in or exceeding a particular damage state (*ds*), given the seismic ground motion. Different measures of the latter can be adopted: the peak ground acceleration, the spectral acceleration, the spectral displacement, etc.. In this study, the spectral displacement is used, assuming a lognormal cumulative distribution for fragility curves [FEMA, 2003]:

$$P[ds \mid S_d] = \Phi\left[\frac{1}{\beta_{ds}} \ln\left(\frac{S_d}{\overline{S}_{d,ds}}\right)\right] \tag{2}$$

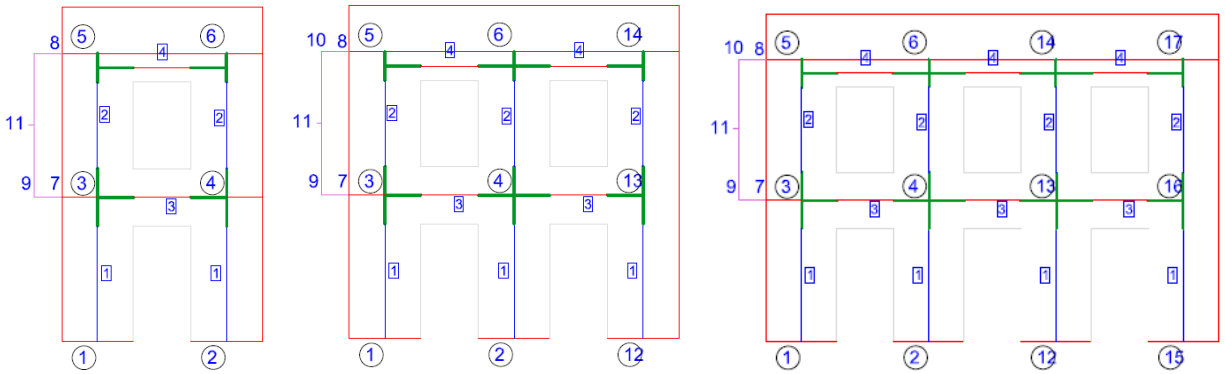

a) 2S1B b) 2S2B c) 2S3B

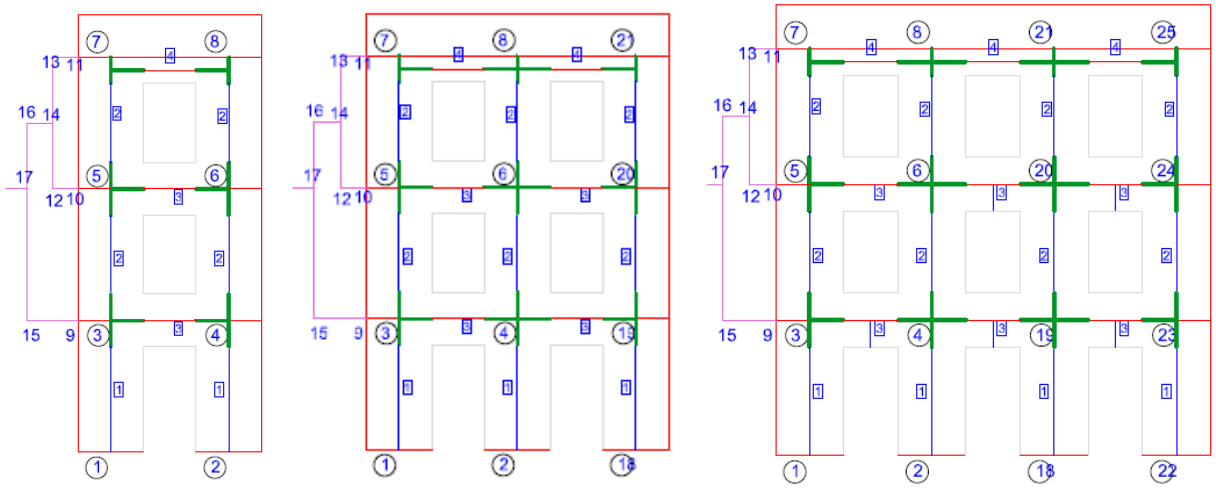

d) 3S1B e) 3S2B f) 3S3B

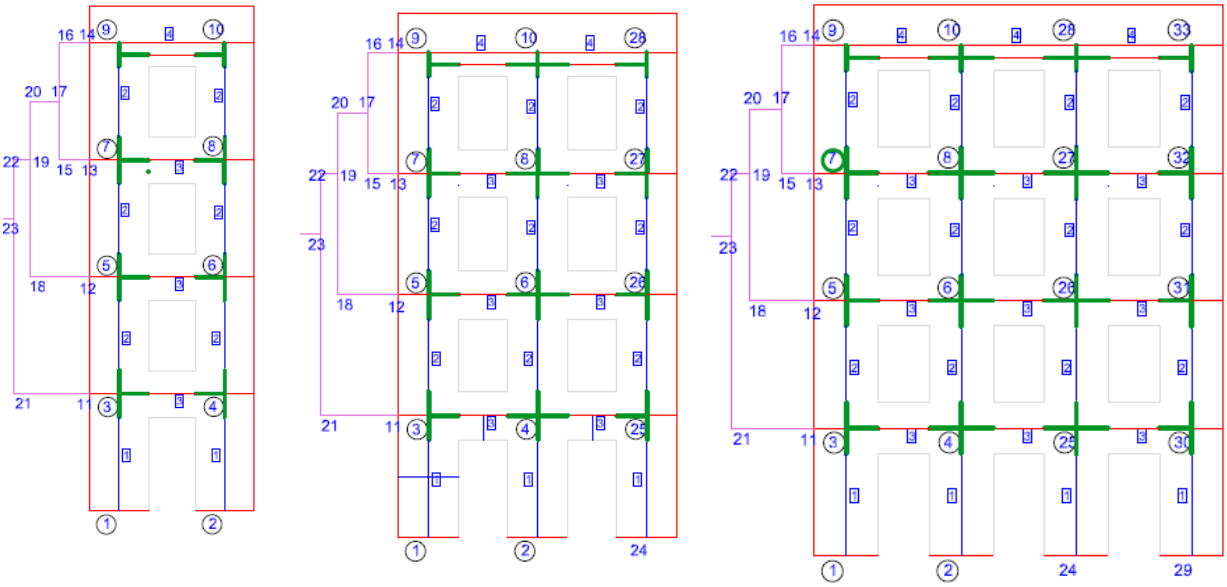

g) 4S1B h) 4S2B i) 4S3B

Figure 10: Equivalent frame model of prototype wall models.

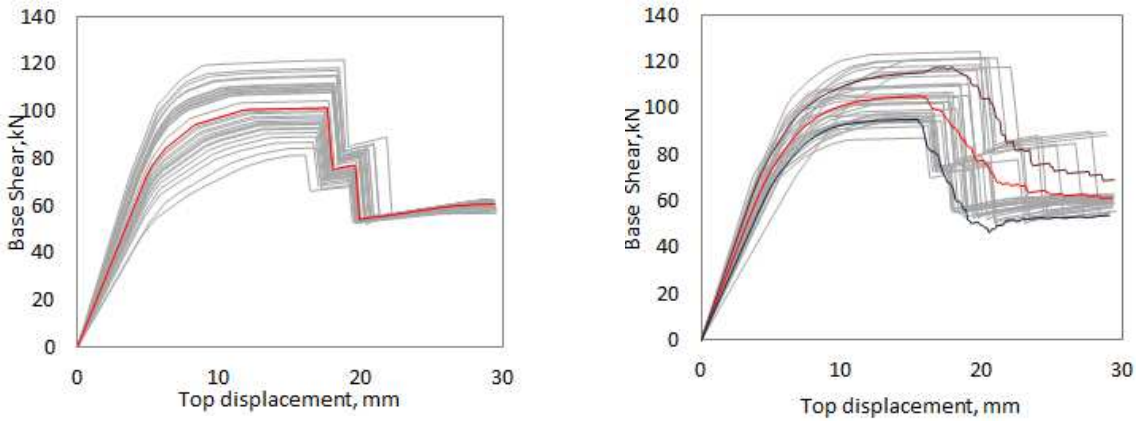

a) Correlated distributions

b) Uncorrelated distributions

Figure 11: Pushover curves for 2S2B wall for correlated and uncorrelated distributions of mechanical properties.

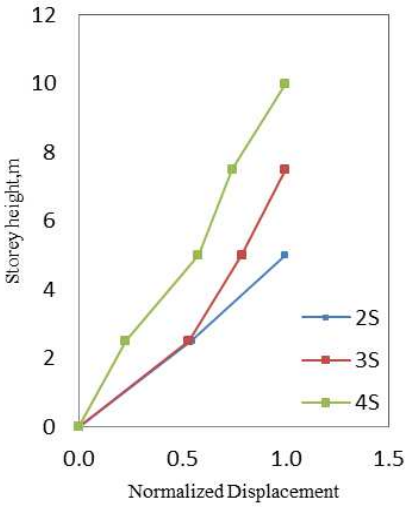

Figure 12: Displacement shapes normalized to top displacement.

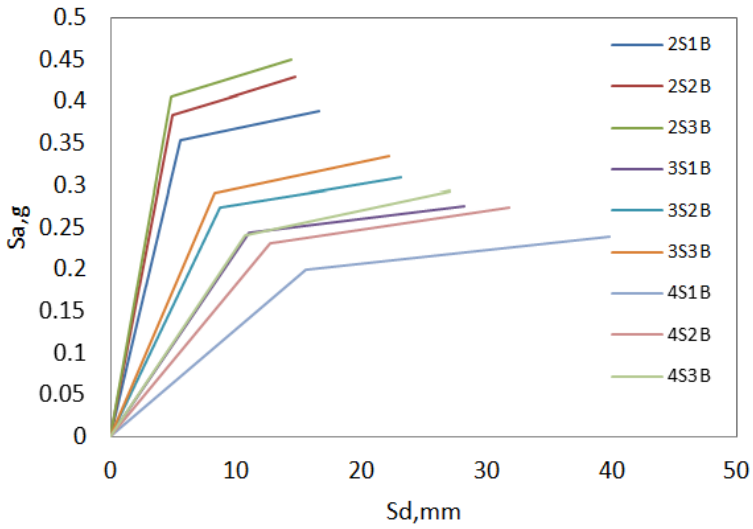

Figure13: Set of idealized bilinear capacity spectrum curves.

Model	S_{dy} (mm)	S_{ay} (g)	S_{du} (mm)	S_{au} (g)
2S1B	5.54	0.353	16.63	0.389
2S2B	4.90	0.383	14.67	0.429
2S3B	4.85	0.405	14.33	0.450
3S1B	11.00	0.244	28.19	0.275
3S2B	8.75	0.274	23.17	0.310
3S3B	8.30	0.290	22.24	0.335
4S1B	15.54	0.199	39.79	0.239
4S2B	12.70	0.231	31.84	0.273
4S3B	10.76	0.293	27.04	0.293

Table 3: Points of idealized bilinear curves.

where, $\overline{S_{d,ds}}$ is the median value of the spectral displacement corresponding to damage state *ds* and β_{ds} its standard deviation. The parameter β_{ds} describes the total variability of the fragility curve for a given damage state and depends on the variability associated with the capacity curve β_C, the demand spectrum β_D and the discrete threshold of the damage state $\beta_{M(ds)}$, and is given by:

$$\beta_{ds} = \sqrt{(CONV[\beta_C \beta_D])^2 + (\beta_{M(ds)})^2} \tag{3}$$

The HAZUS method was originally developed as a tool for estimating seismic scenarios corresponding to a given earthquake; it was later adapted for estimating the loss according to the Probabilistic Seismic Hazard Assessment (PSHA), i.e. considering the occurrence of all possible earthquakes [FEMA, 2003]. In this case the dispersion of the demand is already modelled in the PSHA and shall be removed from the seismic fragility curves to avoid counting it twice; the dispersion becomes accordingly:

$$\beta_{ds} = \sqrt{(\beta_C)^2 + (\beta_{M(ds)})^2} \tag{4}$$

Dispersion values are provided by HAZUS for low rise URM buildings as function of the degradation of the structural system (Table 4).

Capacity curve variability β_C	**Degradation of structural system**								
	Minor			Major			Extreme		
	Damage variability $\beta_{M(ds)}$			Damage variability $\beta_{M(ds)}$			Damage variability $\beta_{M(ds)}$		
	Small (0.2)	Mod (0.4)	Large (0.6)	Small (0.2)	Mod (0.4)	Large (0.6)	Small (0.2)	Mod. (0.4)	Large (0.6)
Very small (0.1)	0.70	0.80	0.90	0.85	0.90	1.00	0.95	1.00	1.10
Small (0.2)	0.70	0.80	0.90	0.85	0.90	1.00	0.95	1.05	1.15
Moderate (0.3)	0.75	0.80	0.95	0.85	0.95	1.05	1.00	1.05	1.15
Large (0.4)	0.80	0.80	0.95	0.90	1.00	1.10	1.05	1.10	1.20

Table 4: Dispersion β_{ds} for URM buildings with degradation [FEMA, 2003].

The damage states can be defined: a) as quantities, local or global, relevant to the model response, or b) from the bilinearized capacity curve.

In the first case the damage states are associated with the achievement of predefined values of drift or characteristic points of the capacity curve. We considered four states of damage, or limit states. The Immediate Occupancy (IO) limit state is characterized by the achievement of 0.1% drift. The Damage Limit State (DLS) corresponds to the achievement of 0.2% drift. The third and fourth limit states are associated with the global response, as determined by the capacity curve. The Life Safety (LS) limit state is associated with the maximum base shear and the Collapse Prevention (CP) limit state with the 20% drop of base shear, compared to the maximum.

It can be observed that the 20% drop of base shear always occurs in coincidence with the attainment of the maximum. Therefore, for the models analyzed, the LS and CP limit states

coincide. The pushover curves for the different models, indicating the limit states, are shown in Figure 14, where the horizontal axis reports the mean value of the spectral displacement over the building population. The mean values of the spectral displacement for the different limit states are also given in Table 5 and Figure 15 for each model. It can be noticed that bay's number has negligible effect on the IO and DLS limit states. On the contrary, its influence is significant on the limit state LS. The fragility curves calculated according to this method are shown in Figure 16.

Damage state	2S1B	2S2B	2S3B	3S1B	3S2B	3S3B	4S1B	4S2B	4S3B
IO	3.842	3.704	3.674	6.091	5.527	5.229	7.272	6.969	6.557
DLS	7.671	7.536	7.394	11.685	11.821	11.972	14.304	14.508	14.562
LS	13.701	12.689	12.243	23.256	20.533	19.258	30.377	25.942	22.842

Table 5: Mean spectral displacements for the different limit states [in mm].

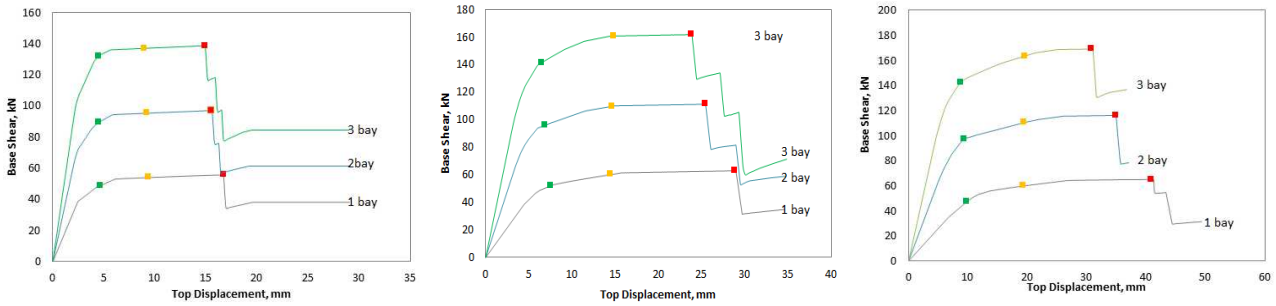

a) 2 stories b) 3 stories c) 4 stories

Figure 14: Median pushover curves with indication of the damage states.

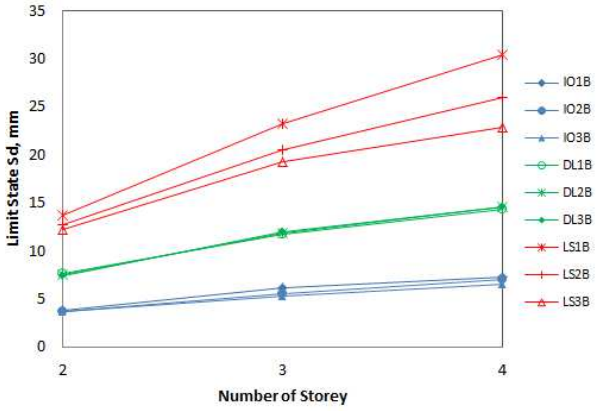

Figure 15: Mean spectral displacements.

The second method [Barbat *et al.*, 2006], [Giovinazzi, 2005], [Kappos *et al.*, 2002] operates on the bilinearized capacity curves. These are calculated on the basis of the median values of yielding acceleration and ultimate displacement. In this study, we adopt the definitions of the mean values corresponding to the damage states proposed by [Kappos *et al.*, 2002] yielding to the results reported in Table 6. The fragility curves obtained according to this method are shown in Figure 17.

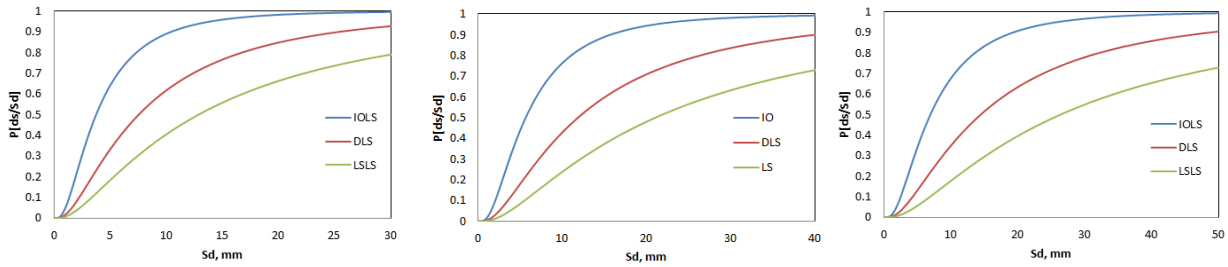

a) 2 stories b) 3 stories c) 4 stories

Figure 16: Fragility curves for URM walls (method a).

Damage state	2S1B	2S2B	2S3B	3S1B	3S2B	3S3B	4S1B	4S2B	4S3B
DS1	4.71	4.17	4.12	9.35	7.44	7.06	13.21	10.80	9.15
DS2	8.31	7.35	7.28	16.50	13.13	12.45	23.31	19.05	16.14
DS3	11.36	10.03	9.87	20.87	16.86	16.08	29.47	23.84	20.23
DS4	14.14	12.47	12.18	23.97	19.69	18.91	33.83	27.07	22.99

Table 6: Median damage state value [in mm].

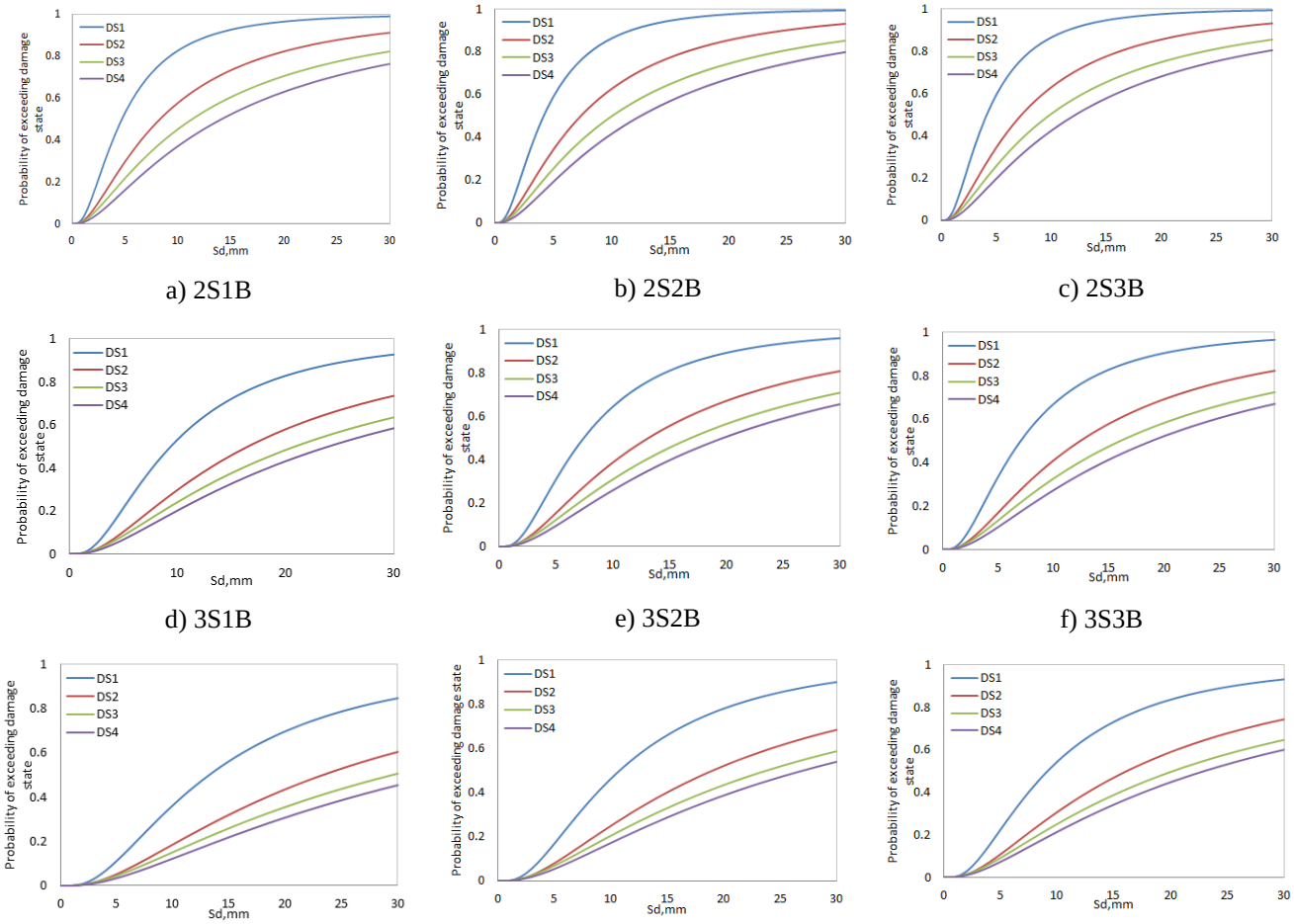

a) 2S1B b) 2S2B c) 2S3B

d) 3S1B e) 3S2B f) 3S3B

g) 4S2B h) 4S2B i) 4S3B

Figure 17: Fragility curves for URM walls (method b).

5 CONCLUSIONS

This study presents the evaluation of the seismic vulnerability of existing URM buildings of Kathmandu Valley, based on fragility curves and the capacity spectrum method.

A set of prototype walls has been defined on the basis of a Rapid Visual Screening. The prototype walls represent not only the buildings in the surveyed area, but also other historical areas of Kathmandu Valley. A Monte Carlo simulation has been performed for the prototype walls under in-plane seismic actions varying the mechanical properties of masonry.

The prototype walls have been analyzed according to the equivalent frame model. Piers and spandrels are modelled with a central Timoshenko beam element, flexural hinges at the ends and a shear link with elastic-perfectly plastic behaviour. The node zones are modelled by means of rigid offsets. The comparison of the model with the experimental results of the full scale prototype tested at Pavia University showed a good agreement, both in terms of pushover curve and failure mechanism. The equivalent frame model results particularly suited for Monte Carlo simulation thanks to its small computational burden and its satisfying accuracy.

The fragility curves of the prototype URM walls have been derived through a stochastic nonlinear analysis. The uncertainties on the mechanical properties of masonry have been taken into account through Monte Carlo method. The analysis has been performed assuming either correlated or uncorrelated distributions of the mechanical properties. The hypothesis of uncorrelated distributions appears more realistic in describing the post-peak behaviour of the capacity curves.

Finally, the fragility curves have been derived either: a) by defining the damage states through quantities relevant to the model response (drift or capacity curve), or b) by defining the damage states on the bilinearized capacity curve.

ACKNOWLEDGEMENTS

The authors acknowledge the contribution of the European Commission through a PhD fellowship to the first author within the EU-NICE Erasmus Mundus Project.

This study was in part carried out under the programs of the “Dipartimento della Protezione Civile – Consorzio ReLUIS”, signed on 2013-12-27, Research Line Masonry Structures. The opinions expressed in this publication are those of the authors and are not necessarily endorsed by the Dipartimento della Protezione Civile.

REFERENCES

[1] Pradhan BK (2007) Disaster preparedness for natural hazards: current status in Nepal. International Centre for Integrated Mountain Development (ICIMOD), Kathmandu, Nepal.

[2] United Nations Office for the Coordination of Humanitarian Affairs (OCHA) (2013) Nepal: Preparing for an earthquake in the Kathmandu Valley. http://www.unocha.org/top-stories/all-stories/nepal-preparing-earthquake-kathmandu-valley.

[3] Jain SK (1998) Lessons from recent Indian earthquakes. Editorial as Guest Editor of Special Issue on Earthquakes in India. Indian Concrete Journal, 72(11).

[4] Kathmandu Valley earthquake risk management project (KVERMP) (1999) Geohazards International, http://geohaz.org/projects/kathmandu.html.

[5] Japan International Cooperation Agency (JICA), Ministry of Home Affairs, HMG of Nepal (2002) The study on earthquake disaster mitigation in the Kathmandu Valley, Kingdom of Nepal. Final Report.

[6] Magenes G, Della Fontana A (1998) Simplified non-linear seismic analysis of masonry buildings. Proc. of the 5th International Masonry Conference, London, 190-195.

[7] Penna A, Morandi P, Rota M, Manzini CF, da Porto F, Magenes G. (2014) Performance of masonry buildings during the Emilia 2012 earthquakes. Bull Earthquake Eng, 12(5):2255-2273. http://dx.doi.org/10.1007/s10518-013-9496-6.

[8] Sorrentino L, Liberatore L, Decanini LD, Liberatore D. (2014) The performance of churches in the 2012 Emilia earthquakes. Bull Earthquake Eng, 12(5):2299-2331. http://dx.doi.org/10.1007/s10518-013-9519-3.

[9] Sorrentino L, Liberatore L, Liberatore D, Masiani R. (2014) The behaviour of vernacular buildings in the 2012 Emilia earthquakes. Bull Earthquake Eng, 12(5):2367-2382. http://dx.doi.org/10.1007/s10518-013-9455-2.

[10] Salonikios T, Karakostas C, Lekidis V, Anthoine A (2003) Comparative inelastic pushover analysis of masonry frames. Engineering Structures, 25(12): 1515-1523.

[11] Kappos AJ, Penelis GG, Drakopoulos CG (2002) Evaluation of simplified models for lateral load analysis of unreinforced masonry buildings. ASCE, Journal of Structural Engineering, 128(7): 890-897.

[12] Pasticier L, Amadio C, Fragiacomo M (2008) Non-linear seismic analysis and vulnerability evaluation of a masonry building by means of the SAP2000 V.10 code. Earthquake Engineering and Structural Dynamics, 37(3): 467-485.

[13] Dolce M (1991) Schematizzazione e modellazione degli edifici in muratura soggetti ad azioni sismiche. L'Industria delle Costruzioni 242:44-57.

[14] Addessi D, Liberatore D, Masiani R (2015) Force-based beam finite element (FE) for the pushover analysis of masonry buildings. International Journal of Architectural Heritage, 9(3): 231-243. http://dx.doi.org/10.1080/15583058.2013.768309.

[15] Liberatore D, Addessi D (2015) Strength domains and return algorithm for the lumped plasticity equivalent frame model of masonry structures. Engineering Structures. http://dx.doi.org/10.1016/j.engstruct.2015.02.030.

[16] Calvi GM, Magenes G. (1994) Experimental research on response of URM building systems. In: Abrams DP, Calvi GM (Eds.), Proc. of the U.S.-Italy Workshop on Guidelines for Seismic Evaluation and Rehabilitation of Unreinforced Masonry Buildings. State University of New York at Buffalo, Technical Report NCEER-94-0021, 3-41/57.

[17] Calvi GM, Magenes G (1995) Indagine sperimentale e numerica su un prototipo di edificio in muratura: rapporto sullo sviluppo del progetto. Atti del 7° Convegno Nazionale "L'Ingegneria Sismica in Italia", Siena, 291-300.

[18] FEMA (2002) Rapid Visual Screening of Buildings for Potential Seismic Hazards – A Handbook. FEMA 154. Federal Emergency Management Agency, Washington, DC, U.S.A..

[19] Rota M, Penna A, Magenes G (2010) A methodology for deriving analytical fragility curves for masonry buildings based on stochastic nonlinear analyses. Engineering Structures, 32(5): 1312-1323.

[20] CNR (2014) Istruzioni per la valutazione affidabilistica della sicurezza sismica di edifici esistenti. CNR-DT 212/2013, Consiglio Nazionale delle Ricerche, Roma.

[21] Jaishi B, Ren W-X, Zong Z-H, Maskey PN (2003) Dynamic and seismic performance of old multi-tiered temples in Nepal. Engineering Structures, 25(14): 1827-1839.

[22] Parajuli HR, Kiyono J, Tatsumi M, Suzuki Y, Umemura H, Taniguchi H, Toki K, Furukawa A, Maskey PN (2011a) Dynamic characteristic investigation of a historical masonry building and surrounding ground in Kathmandu. Journal of Disaster Research, 6(1): 26-35.

[23] Parajuli HR, Kiyono J, Maskey PN, Taniguchi H (2011b) Investigations of material properties on old brick masonry buildings of Kathmandu. Disaster Mitigation of Cultural Heritage and Historic Cities, 5.

[24] Parajuli HR, Maskey PN, Taniguchi H (2012) Vulnerability assessment of the old brick masonry buildings. Disaster Mitigation of Cultural Heritage and Historic Cities, 6: 61-66.

[25] Parajuli HR (2012) Determination of mechanical properties of the Kathmandu World Heritage brick masonry buildings. Proc. of the 15th World Conference on Earthquake Engineering, Lisboa.

[26] ATC (1996) Seismic Evaluation and Retrofit of Concrete Buildings. Report ATC-40, Applied Technology Council, Redwood City, California, U.S.A..

[27] FEMA (2003) HAZUS MH MR4. Technical Manual. Federal Emergency Management Agency, Washington, DC, U.S.A..

[28] Barbat, AH, Yépez Moya F, Canas JA (1996) Damage scenarios simulation for seismic risk assessment in urban zones. Earthquake Spectra, 12(3): 371-394.

[29] Giovinazzi S (2005) The vulnerability assessment and the damage scenario in seismic risk analysis, PhD Thesis, Technical University Carolo-Wilhelmina at Braunschweig, Braunschweig, Germany and University of Florence, Florence, Italy.